A time-dependent three-dimensional dayside magnetopause model based on quasi-elastodynamic theory

Yaxin Gu[1,2,3]**, Yi Wang**[1,2]**, Fengsi Wei**[1,2]**, Xueshang Feng**[1,2]**, Andrey Samsonov**[3]**, Xiaojian Song**[4]**, Boyi Wang**[1,2]**, Pingbing Zuo**[1,2]**, Chaowei Jiang**[1,2]**, Yalan Chen**[1,2]**, Xiaojun Xu**[5]**, and Zilu Zhou**[5]

[1]State Key Laboratory of Solar Activity and Space Weather, School of Aerospace, Harbin Institute of Technology, Shenzhen, China
[2]Shenzhen Key Laboratory of Numerical Prediction for Space Storm, School of Aerospace, Harbin Institute of Technology, Shenzhen, China
[3]Mullard Space Science Laboratory, University College London, Dorking, RH56NT, United Kingdom
[4]Shandong Institute of Advanced Technology, Shandong, 250100, China
[5]State Key Laboratory of Lunar and Planetary Sciences, Macau University of Science and Technology, Macau, China

Correspondence: Yi Wang (wingwy@mail.ustc.edu.cn, wy@hit.edu.cn)

Abstract. The interaction between the solar wind and Earth's magnetosphere is a critical area of research in space weather and space physics. Accurate determination of the magnetopause position is essential for understanding magnetospheric dynamics. While numerous magnetopause models have been developed over past decades, most are time-independent, limiting their ability to elucidate the dynamic movement of the magnetopause under varying solar wind conditions. This study introduces the first time-dependent three-dimensional magnetopause model based on quasi-elastodynamic theory, named the POS (Position–Oscillation–Surface wave) model. Unlike existing time-independent models, the POS model physically reflects the dynamic responses of magnetopause position and shape to time-varying solar wind conditions. The predictive accuracy of the POS model was evaluated using 38 887 observed magnetopause-crossing events. The model achieved a root-mean-square error of 0.774 Earth radii (R_E TS1), representing a 17.9 % improvement over five widely used magnetopause models. Notably, the POS model demonstrated superior accuracy under highly disturbed solar wind conditions (22.1 % better) and in higher-latitude regions (27.0 % better) and flank regions (33.3 % better) of the magnetopause. The POS model's remarkable accuracy, concise formulation, and fast computational speed enhance our ability to predict magnetopause position and shape in real time. This advancement is significant for understanding the physical mechanisms of space weather phenomena and improving the accuracy of space weather forecasts. Furthermore, this model may provide new insights and methodologies for constructing magnetopause models for other planets.

1 Introduction

The magnetopause, the boundary between the interplanetary magnetic field (IMF) and Earth's magnetic field, plays a crucial role in space weather forecasting and in understanding solar wind–magnetosphere coupling mechanisms (Willis, 1971; Song et al., 1996; Russell, 2003). It acts as a protective shield against hazardous energetic particles while simultaneously serving as the primary interaction region for solar wind–magnetosphere coupling. The magnetopause exhibits considerable dynamic behaviour due to continuous solar wind variations and various instabilities – even under steady solar wind conditions (Anderson et al., 1968; Song et al., 1988; Eastwood et al., 2015). These dynamics can lead to radiation-belt particle loss, field-aligned current intensification, ultra-low-frequency wave generation, and solar wind energy conversion, which affect the radiation belts, polar regions, and ionosphere (Haerendel, 1990; Mann et al., 2012; Plaschke, 2016; Mottez, 2016; Archer et al., 2019). Conse-

quently, comprehending the interactions between the solar wind and the magnetopause is vital for advancing magnetospheric dynamics and improving space weather prediction capabilities (Feng, 2020; Zong et al., 2020).

Numerous magnetopause models have been established over the past few decades, generally categorized as physical (or principal) models (Ferraro, 1952; Beard, 1960; Spreiter et al., 1966) and empirical models (Fairfield, 1971; Tsyganenko, 1989; Shue et al., 1998; Lin et al., 2010). Physical models are primarily based on the classic Chapman–Ferraro theory proposed in the 1930s (Chapman and Ferraro, 1930), which states that the magnetopause's equilibrium position is determined by the pressure balance between solar wind dynamic pressure (P_{dyn}) and magnetospheric magnetic pressure (P_b). Since the 1960s, the launch of numerous satellites has provided us with a large number of samples of magnetopause-crossing events (MCEs), thereby creating the possibility for the establishment of empirical models (Fairfield, 1971; Sibeck, 1991; Petrinec and Russell, 1996; Shue et al., 1998; Lin et al., 2010). Many empirical models rely on two key parameters, P_{dyn} and IMF B_z, and some models use the Earth's dipole tilt angle (Φ) to calibrate the higher-latitude zone. Besides, some empirical models proposed in the 1980s combine physical processes of solar wind–magnetosphere interactions with satellite observation fitting and involve the impact of the magnetospheric current system (Tsyganenko, 1989; Tsyganenko and Stern, 1996). Regardless of the assumptions on which these models are based, all these models have contributed to our understanding of magnetopause movement and its response to solar wind conditions. In particular, many of them have been widely used in the prediction of the magnetopause due to their simple form and high prediction accuracies.

However, it should be stated that these models primarily describe the average steady-state characteristics of the magnetosphere. To accurately describe the dynamic coupling process of solar wind–magnetosphere interaction, it is essential to incorporate time-partial derivatives into dynamic equations (Smit, 1968; Petrinec, 2001; Borovsky and Alejandro Valdivia, 2018). This approach, however, complicates the solution of model equations, often necessitating numerical simulations such as magnetohydrodynamics (MHDs)**CE1** (Powell et al., 1999; Raeder et al., 2001; Lyon et al., 2004; Tóth et al., 2005; Merkin and Lyon, 2010), particle-in-cell (PIC) (Moritaka et al., 2012; Ashida et al., 2014; Walker et al., 2019), and hybrid simulations (Gargaté et al., 2008; Omelchenko et al., 2021; Ala-Lahti et al., 2022). Numerical simulations are widely used in exploring solar wind–magnetosphere coupling and can accurately reveal the position of the magnetopause changing with the time-varying solar wind conditions. Collado-Vega et al. (2023) compared the magnetopause predictions obtained from different MHD models, showing the discrepancies in the standoff position. Their analysis also specifically addressed the impact of extreme solar wind conditions, which are known to cause space weather hazards, on the magnetopause. However, the introduction of time-partial derivatives makes equations very difficult to solve. Additionally, many prominent numerical simulation models may not properly include all magnetospheric current systems (e.g. the ring current or the magnetospheric–ionospheric currents); therefore, this omission may result in systematic errors in the magnetopause prediction (Samsonov et al., 2016). Moreover, numerical models are solved on supercomputers, consuming a significant amount of computing resources and time, rendering them impractical for real-time space weather forecasting (Raeder et al., 2001; Lyon et al., 2004; Tóth et al., 2005; Feng, 2020). This limitation highlights the need for more efficient yet accurate magnetopause models that can capture the dynamic nature of the magnetopause while remaining computationally feasible for real-time applications. Such models would significantly enhance our ability to predict and understand space weather phenomena, bridging the gap between theoretical understanding and practical forecasting capabilities.

Figure 1. The schematic diagram of time-independent **(a)** and time-dependent **(b)** magnetopause models.

Apart from numerical simulations, very few time-dependent magnetopause models have been historically developed (Smit, 1968; Børve et al., 2011; Freeman et al., 1995; Sato et al., 2022). Figure 1 illustrates the fundamental difference between time-independent and time-dependent models. In time-independent models, the magnetopause position is directly correlated with instantaneous solar wind conditions. For example, a step-like increase in solar wind dynamic pressure (such as a shock) corresponds to an immediate step-like compression of the magnetopause (Fig. 1a). However, this simplification fails to capture the real dynamics of the magnetopause. In reality, the magnetopause undergoes a more complex process of compression and recovery, exhibiting oscillatory characteristics in response to abrupt changes in solar wind conditions, as shown in Fig. 1b (Freeman and Farrugia, 1998; Hu et al., 2005; Desai et al., 2021). Time-dependent models aim to capture these dynamic processes, providing a more accurate representation of magnetopause behaviour. To describe these dynamic responses, it is necessary to incorporate time-partial derivatives into the governing equations. However, this inclusion significantly complicates the solution process. Consequently, existing time-dependent models are predominantly one-dimensional and remain in a preliminary stage of development.

Smit (1968) conceptualized the magnetopause as a rigid surface and attempted to explain its motion from the perspective of periodic vibration; Freeman et al. (1995) investigated the influence of inertial and damping effects on the magnetosphere, employing magnetohydrodynamics to analyse the magnetopause motion; and Børve et al. (2011) set up a non-adjustable model to analyse the oscillation period of the magnetopause. By investigating the movement of the subsolar point in response to time-varying solar wind conditions, these models are primarily constructed to elucidate specific physical phenomena linked to solar wind–magnetosphere interaction, yet they lack the capability to provide a real-time depiction of the three-dimensional magnetopause position and shape.

Hence, the challenge of constructing time-dependent models lies in balancing the need for accurate dynamic representation with computational feasibility. Although time-dependent models offer a more realistic depiction of magnetopause behaviour, their complexity has limited their development and application, particularly in three-dimensional space. This highlights the necessity for new strategies that can capture time-dependent dynamics while ensuring practical utility for computation, especially for real-time space weather forecasting and related magnetospheric research. Previously, our work revealed the quasi-elastodynamic processes involved in the interaction between the solar wind and the magnetosphere (Gu et al., 2023). It suggests that the dynamic behaviour of each point on the magnetopause can be viewed as an equilibrium position (P), as radial global oscillations around the equilibrium position (O), and as a surface-wave-like structure around the flank regions (S). This work offers a practical framework for developing a time-dependent three-dimensional magnetopause model.

However, our previous work primarily focused on elucidating the quasi-elastic process, with less emphasis on the outcomes of model predictions (Gu et al., 2023). Key factors influencing magnetopause dynamics, such as the IMF B_z and Earth's dipole tilt angle (Φ), were not incorporated. Additionally, the adjustable parameters in the equations were simply chosen and lacked thorough calibrations. Moreover, our prior work and most published magnetopause models (Petrinec and Russell, 1996; Shue et al., 1998; Gu et al., 2023) relied on a relatively limited dataset of low-latitude satellite observations, leading to constraints in accurately representing the higher-latitude and flank regions of the magnetopause. To address these limitations and overcome the inherent shortcomings of time-independent models, particularly their inability to reflect the dynamic responses of the magnetopause position and shape to time-varying solar wind conditions, we propose a time-dependent three-dimensional magnetopause model. This model, which has been tested with the largest dataset of MCEs to date (38 887 events), demonstrates remarkable prediction accuracy compared to those of five widely used magnetopause models. Besides, it offers unparalleled real-time computation speed and a concise form relative to numerical simulations. We have named this model the position–oscillation–surface wave (POS) model.

2 Datasets and other magnetopause models for comparison

The THEMIS (Time History of Events and Macroscale Interactions during Substorms) mission (Angelopoulos, 2008), which consists of five spacecraft launched into similar elliptical, near-equatorial orbits in 2007, has significantly enhanced our ability to observe the magnetosphere. The mission provides high-resolution (~ 3 s) magnetic field measurements through the THEMIS/Fluxgate Magnetometer (FGM) (Auster et al., 2008) and plasma data from the THEMIS/Electrostatic Analyser (EA) (McFadden et al., 2008). The CLUSTER II mission (Escoubet et al., 2001), involving four identical spacecraft launched in 2000, also offers high-resolution (~ 4 s) magnetic field measurements using the CLUSTER/Fluxgate Magnetometer (FGM) (Balogh et al., 1997), particle data, and moments from the CLUSTER Ion Spectrometry-Hot Ion Analyser (CIS–HIA) (Rème et al., 1997).

The WIND spacecraft, launched into orbit around Earth in 1994 and relocated to the Lagrange L1 point after 2004, provides continuous, high-quality in situ solar wind observations. This study utilizes high-resolution (~ 3 s) plasma data from the WIND/3D Plasma Analyzer (3DP) (Lin et al., 1995) and magnetic field data from the Magnetic Fields Investigation (MFI) (Lepping et al., 1995) for upstream solar wind observations. For this study, we have compiled a dataset consisting of 51 590 THEMIS MCEs and 38 321 CLUSTER MCEs. After excluding redundant crossings (i.e. those occurring simultaneously on the same satellite), invalid data (i.e. crossings without valid upstream solar wind observations), and nightside MCEs (where $X_{\mathrm{GSM}} < 0$ R_{E}), 38 018 THEMIS MCEs and 869 CLUSTER MCEs (see Fig. 2) are selected for this study. The time shift from (δt) WIND and the satellite MCE is determined by comparing the time of each crossing (t_1) with the probable arrival time of the corresponding solar wind observation from WIND ($t_0 + \delta t$), satisfying $(t_0 + \delta t) - t_1 < 300$ s. The 300 s threshold is set as the potential error window for the time shift from L1 to the magnetopause. δt, calculated as $(\mathrm{L1} - r)/ \langle v_x \rangle$, L1 (L1 $= 235$ R_{E}), is the distance from the Earth to the L1 point, r denotes the radial position of the magnetopause, and $\langle v_x \rangle$ is the 1 h sliding average of the solar wind velocity in the x component (Chao et al., 2002). A summary of these events is provided in Table 1. The distribution of matched solar wind conditions for MCEs is shown in Fig. 3. All data are available in the CDAWeb database (http://cdaweb.gsfc.nasa.gov/, last access: 24 July 2024), and the time resolutions of both the magnetic field and plasma data used in the study are interpolated to a 3 s resolution, set in GSM coordinates.

Table 1. Summary of 89 911 satellite MCEs and datasets used in this paper.

Dataset	Satellite	Time interval	Number of datasets
Song et al. (2021)	THEMIS	2007–2022	17 647
Staples et al. (2020a)	THEMIS	2007–2016	33 943
Grimmich et al. (2024)	CLUSTER	2001–2020	38 321
In this paper	THEMIS/CLUSTER	2004–2022	38 887
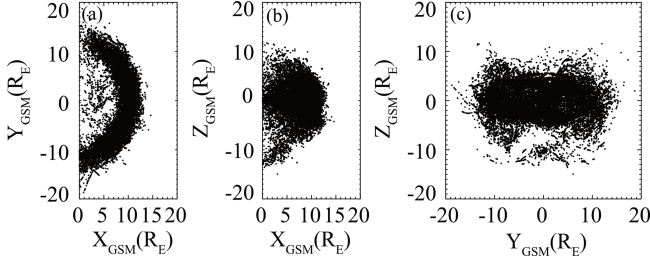
Figure 2. Projections of 38 887 MCEs in the GSM coordinate **(a)** X–Y plane, **(b)** X–Z plane, and **(c)** Y–Z plane.

In previous research on time-independent magnetopause models, the physical models (Ferraro, 1952; Beard, 1960; Spreiter et al., 1966), although theoretically grounded, usu­ally oversimplify intricate solar wind–magnetosphere inter­
5 actions to facilitate calculations, usually without demon­strating apparent higher prediction accuracies compared to widely used empirical models (Petrinec and Russell, 1996; Shue et al., 1997; Shue et al., 1998; Chao et al., 2002; Lin et al., 2010). Hence, this article concentrates on comparing sev­
10 eral notable time-independent empirical models renowned for their superior prediction accuracies (Petrinec and Rus­sell, 1996; Shue et al., 1997; Shue et al., 1998; Chao et al., 2002; Lin et al., 2010).

Empirical models are typically constructed using satellite
15 observations of MCEs. While these models vary in their use of satellite datasets, parameters considered, coordinate sys­tems employed, and functions applied, most are parameter­ized using the dynamic pressure (P_{dyn}) and the interplan­etary magnetic field B_z component (IMF B_z). For exam­
20 ple, Petrinec and Russell (1996) (hereafter PR96) employed an ellipsoidal function to construct a magnetopause model, while Shue et al. (1997) (hereafter S97) developed a flexi­ble function incorporating two variables: the subsolar mag­netopause position (R_0) and the tail flaring angle (α). This
25 function has gained widespread use as a foundational ap­proach to describing magnetopause shape. For instance, Shue et al. (1998) (hereafter S98) accounted for the saturation ef­fect of the IMF B_z on R_0, and Chao et al. (2002) (hereafter C02) extended their model for application under normal and
30 extreme solar wind conditions.

Nevertheless, these models primarily rely on low-latitude satellite observations and may not adequately capture the dis-
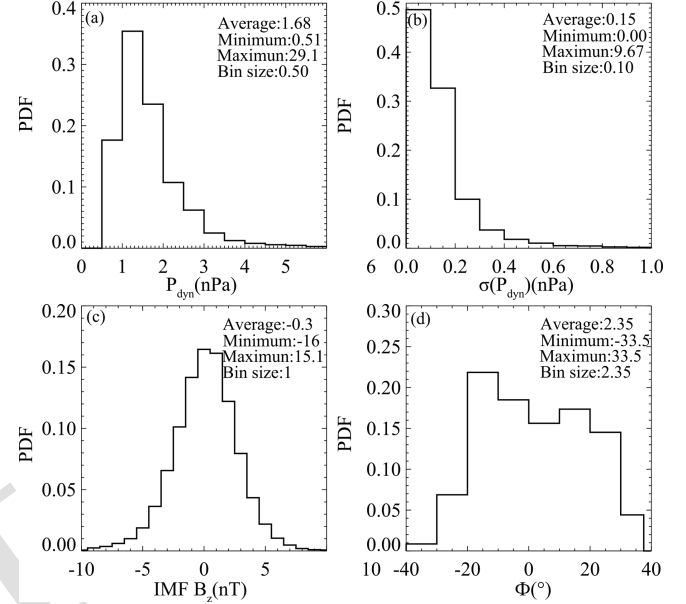
Figure 3. Probability density function of upstream solar wind ob­servations in terms of **(a)** the solar wind dynamic pressure (P_{dyn}), **(b)** the standard deviation of dynamic pressure (P_{dyn}), **(c)** the in­terplanetary magnetic field B_z component (IMF B_z), and **(d)** the dipole tilt angle (Φ).

tinctive characteristics of the magnetopause in the higher-latitude region. Besides, they are constructed with the P_{dyn} and the IMF B_z, while it is found that the dipole tilt angle Φ is 35 of great significance when modelling the magnetopause, es­pecially in the higher-latitude region. Formisano et al. (1979) constructed an average magnetopause size and shape for two dipole tilt angle values (Φ). Boardsen et al. (2000) devel­oped a higher-latitude magnetopause model parameterized 40 not only by the P_{dyn} and the IMF B_z but also by the dipole tilt angle (Φ), recognizing its significant influence on the shape of the higher-latitude region of the magnetopause. While this model is specifically designed for higher-latitude regions, it is not as effective in accurately calculating the magnetopause 45 at low latitudes compared to other models due to inherent limitations.

The above models are generally developed under the as­sumption of axial symmetry, while the actual magnetopause shape is asymmetrical in both the Y and Z directions, so they 50 are essentially 2D or 2.5D models. To describe the 3D struc-

Table 2. Summary of five widely used magnetopause models and the POS model.

Model name	Number of higher-latitude MCEs used	Time range of MCEs used	Dimensions
PR96	1147	1979–1980	2D/2.5D
S97	553	1978–1986	2D/2.5D
S98	553	1978–1986	2D/2.5D
C02	552	1978–1986	2D/2.5D
L10	1226 (1482)	1994–2008	3D
POS	31 562 (7325)	2004–2022	3D

ture of the magnetopause, Lin et al. (2010) (hereafter L10) developed a three-dimensional magnetopause model parameterized by the P_{dyn}, the thermal pressure (P_t), the IMF B_z, and the Φ. The coordinate systems employed in these empirical models are typically comprised of aberrated coordinates, which account for Earth's orbital motion (Petrinec and Russell, 1996; Shue et al., 1997; Shue et al., 1998; Chao et al., 2002), or corrected coordinates which compensate for both Earth's orbital motion and deviations in solar wind velocity from the Sun–Earth line (Boardsen et al., 2000; Lin et al., 2010). A summary of the five widely used magnetopause models is presented in Table 2.

3 The POS model

In our previous work (Gu et al., 2023), we modelled the compression–recovery process of the magnetopause as a quasi-elastodynamic phenomenon. In this framework, the dynamic pressure, $P_{dyn} = n_{sw} m_p v_x^2$, serves as the driving force on the system, where n_{sw}, m_p, and v_x are the number density, proton mass, and x component of the solar wind velocity in GSM coordinates, respectively. The system's restoring force is described by $P_b = B^2/2\mu_0$, where B is the total magnetic field at the magnetopause and μ_0 is the vacuum permeability. After accounting for damping and non-ideal effects, P_{damp}, and excluding the complex coupling interactions, the momentum equation for the magnetosheath in a unit cylinder can be represented by Eq. (1).

$$M_{msh} a_{msh} = P_b - P_{dyn} - P_{damp} \tag{1}$$

Given that the derivation process of the foundational formula is the same as our previous work and that this paper is focused on model predictions rather than physical processes, we will refrain from reiterating it here. The relationship depicting the temporal evolution of the magnetopause position (r) is introduced in Eq. (2):

$$n_{sw} m_p r \ddot{r} = \frac{(\lambda \boldsymbol{B}_d(r, \theta, \varphi) + \boldsymbol{B}_c(r))^2}{2\mu_0}$$
$$- n_{sw} m_p \boldsymbol{v}_x^2 \cos^2\alpha - k \Sigma_p \boldsymbol{B}_p^2 \dot{r} - \eta \dot{r}/r, \tag{2}$$

where r, θ, and ϕ represent the corresponding spherical coordinates. The variable r is the radial distance; θ is the latitude angle in the range $[-90°, 90°]$; and φ is the longitude angle, adjusted to the range $[-180°, 180°]$ with $0°$ oriented towards the Sun for simplicity – all the vectors have been projected to the normal direction of the magnetopause (Gu et al., 2023). This simplified equation enables us to capture the fundamental dynamics of the magnetopause's response to solar wind fluctuations while ensuring computational efficiency. The first term on the right side of Eq. (2) signifies the restoring force P_b. Here, B_d denotes the Earth's dipole field, λ is the magnetospheric compressibility coefficient, and B_c accounts for contributions from various magnetospheric currents. The second term on the right side represents the driving force P_{dyn}, where α denotes the angle between the x direction and the normal direction of the magnetopause. The third term on the right side of Eq. (2) characterizes a position-dependent dragging effect estimated from the ionosphere. The fourth term illustrates a global non-ideal viscous effect. B_p is the estimated ionospheric magnetic field in the polar region, Σp stands for the equivalent Pederson conductivity, k serves as a position-dependent mapping factor, and η represents the viscous coefficient. The final two terms contribute to the damping and non-ideal effects of the system, denoted as P_{damp}. Equation (2) provides a foundation for developing a time-dependent magnetopause model that can reflect the system's dynamic behaviour more accurately compared to conventional time-independent models. We will introduce the key parameters in detail in the following sections. All the parameters are in SI units.

In this study, we incorporate the impact of IMF B_z and Φ in the magnetospheric magnetic pressure. To determine the equation's final fitting coefficients, we conducted 1000 independent iterations, each involving a random selection of 5000 MCEs from our dataset of 38 887 MCEs.

3.1 The magnetospheric compressibility coefficient (λ)

The magnetospheric compressibility coefficient, λ, measures the magnetosphere's response to solar wind pressure, specifically the ratio of the magnetospheric magnetic field to the pure dipolar magnetic field (Spreiter et al., 1966; Schield, 1969). This coefficient is one of the most critical parameters directly affecting the position of the magnetopause. Typically, λ has a value of 2.44 at the subsolar point, but it changes as the magnetopause shifts and varies with latitude and longitude, suggesting a more complex formulation (Shue et al., 2011; Chen et al., 2023). Mead and Beard (1964) used a self-consistent method and discovered an inward-concave structure at the higher-latitude magnetopause, which is influenced by the inclination angle of Earth's dipole. Their work also determined the surface shape of the magnetopause when the solar wind flow is perpendicular to the dipole axis ($\Phi = 0°$), providing an expression for λ as a function of the angles θ and φ.

Several models (Formisano et al., 1979; Boardsen et al., 2000; Lin et al., 2010) have been developed to investigate the influence of Φ (the angle between Earth's magnetic axis and the solar wind direction) on the magnetopause's position and shape, offering valuable insights into the magnetosphere's three-dimensional structure. These models predict an asymmetrical response of the magnetosphere to variations in Φ. Boardsen et al. (2000) quantified the effects of Φ on the higher-latitude region of the magnetopause using MCE data from the Northern Hemisphere. Their work revealed how the dipole tilt angle influences the magnetopause structure in polar regions, which are particularly sensitive to changes in the orientation of Earth's magnetic field relative to the solar wind. Lin et al. (2010) further demonstrated that an increase in Φ causes a slight shift in the centres of the magnetopause cross-sections, moving them towards the negative Z direction in the subsolar region and towards the positive Z direction in the tail region. According to Olson (1969), who provided a detailed representation of λ for various tilt angles ($\Phi = 0, 10, 20, 30°$) on a $15° \times 15°$ grid of θ and φ values, the dipole tilt angle significantly alters the fundamental behaviour of λ, with varying effects on θ and φ. This influence is more pronounced in higher-latitude regions ($\theta > 30°$). Building on previous work by Gu et al. (2023), in which $\lambda = 2.44 - 0.4\theta^2 + \varphi^2$, we incorporate the effect of Φ on different positions of the magnetopause $\lambda(\theta, \varphi)$ and derive a more precise expression for λ, specifically tailored to our model, as presented in Eq. (3):

$$A = \tanh[5.568(|\theta| - 0.5325)] + 1.0$$
$$\lambda(\theta, \varphi, \Phi) = 2.44 - (0.4 + 0.3A)(\theta + 0.2A\Phi)^2$$
$$+ (1.0 - 0.5A|\Phi|)\varphi^2. \qquad (3)$$

3.2 Contributions from various magnetospheric currents (B_c)

Previous studies on the impact of magnetospheric currents on the position of the magnetopause led to the development of a static magnetopause current model, where the magnetic fields of the magnetopause surface currents and tail currents were fitted using polynomials to reveal the relationship between variations in the magnetospheric magnetic field and changes in magnetopause position, e.g. $B_{surf}(r, \theta, \varphi)$ and $B_{tail}(r, \theta, \varphi)$ (Choe and Beard, 1974a, b; Matsuoka et al., 1995). In our earlier study (Gu et al., 2023), the magnetic field of the current system, denoted as $B_{c0}(r)$, did not account for variations in θ and ϕ. This limitation is addressed in the present study. The fundamental form of $B_{c0}(r, \theta, \phi)$, incorporating these angular dependencies, is introduced in Eq. (4). The current system exhibits asymmetrical effects consistent with other models such as T96 and T01 (Tsyganenko, 2001; Tsyganenko and Stern, 1996). These models also incorporate dawn–dusk asymmetry in the magnetospheric current, reflecting the influence of these angular dependencies.

$$B_{c0}\,\text{TS3}\,(r) = [-401\,904/\left(\frac{r}{R_E}\right)^4 + 65\,489/\left(\frac{r}{R_E}\right)^3$$
$$+ 1500/\left(\frac{r}{R_E}\right)^2 - 40][1 + 0.4\sin(2\theta)^2]$$
$$[1.0 - 0.1\sin(\varphi)] \times 10^{-9} \qquad (4)$$

In our previous work, $B_c(r)$ was defined as a piecewise function of P_{dyn}, which could yield discontinuous and nonphysical results at the transition points (Gu et al., 2023). To address this limitation, we now consider the impact of P_{dyn} in a continuous form, eliminating the piecewise dependence. Furthermore, the impact of the IMF B_z on the magnetopause position is directionally dependent, with a southward IMF triggering dayside magnetic reconnection, an essential process already incorporated in most existing models (Aubry et al., 1970; Dungey, 1961; Fairfield, 1971). To quantify this effect, we adopt a hyperbolic tangent function, similar to that used in Shue et al. (1998). Finally, by considering the combined effects of both IMF B_z and P_{dyn}, B_c is expressed as follows in Eq. (5):

$$B_c = B_{c0}(r, \theta, \varphi)f(B_z)f(P_{dyn})$$
$$= B_{c0}(r)\,\text{TS4}\,[1.0 + 0.2\tanh(-0.5(B_z + 2.5))]$$
$$[1 + 0.1P_{dyn}]. \qquad (5)$$

This formulation of B_c provides a more refined and physically accurate depiction of the influence of the magnetospheric current system on magnetopause dynamics. By incorporating the dependence of the B_c on the IMF B_z and the P_{dyn} and specific locations on the magnetopause, the expression captures the complex spatial variations in the magnetospheric current system that contribute to magnetic pressure, making our model fully three-dimensional.

3.3 The damping items

The damping terms in our model consist of a position-dependent dragging effect from the ionosphere $F_d = k\Sigma_p B_p^2 \dot{r}_{mp}$ and a global non-ideal viscous effect $F_N = \eta\dot{r}_{mp}/r_{mp}$, consistent with our previous work (Chen and Wolf, 1999; Wang and Chen, 2008; Gu et al., 2023). We set $B_p = 3 \times 10^{-5}\,T$ to represent the approximate ionospheric magnetic field in the polar region, while $\Sigma p = 3.4\,S$ serves as the equivalent Pedersen conductivity. The viscous coefficient is artificially set to $\eta = 2 \times 10^{-8}$. As defined in Eq. (6), the position-dependent mapping factor k is empirically calibrated based on the magnetopause location (r, θ, φ), increasing when the magnetopause compresses and decreasing with increasing latitude and longitude.

$$k = [196(0.05 + e^{-0.05(r/R_E)^2}) - 3.2|\theta| - 1.6|\varphi|] \times 10^{-7} \qquad (6)$$

4 Results

By substituting the relevant parameters into Eq. (2) and assuming the initial shape of the magnetopause as a paraboloid, $x = -0.03(y^2 + z^2) + R_0$, where R_0 is determined by the
5 pressure balance at the subsolar point. The position of each point on the magnetopause can be computed instantaneously on a personal computer. The prediction accuracies of the POS model and other notable time-independent models mentioned earlier are evaluated and compared with MCEs at the
10 real THEMIS location. Prediction accuracy is quantified using the root-mean-square error (RMSE) `TS5`, calculated between model outputs and their corresponding MCE observations. A dataset of 38 887 MCEs observed by the THEMIS and CLUSTER satellites is used for testing. To evaluate the
15 performance of the POS model relative to the performances of other models, we calculate the ratio $\delta(\Delta)/\Delta_{\text{POS}}$: where $\delta(\Delta)$ represents the difference in RMSE between a previous model and the POS model and Δ_{POS} is the RMSE of the POS model. This comparison is conducted from various perspec-
20 tives. The probability density distributions of RMSE for each model are illustrated in Fig. 4.

It can be seen that all models are capable of adequately predicting magnetopause positions, with the majority (> 70 %) showing RMSE within 1 R_{E}. Our model demon-
25 strates superior accuracy, with 80 % of its prediction errors falling below 1 R_{E}. For the other models, predicting the magnetopause under disturbed solar wind conditions is more challenging, while the POS model shows improved performance in such conditions, with 60 % of predictions remain-
30 ing within 1 R_{E}. Given the inherent asymmetry of the magnetopause, we evaluated the performance of each model in both the flank region ($|\varphi| \geq 60°$) and the higher-latitude region ($|\theta| \geq 30°$). The POS model consistently outperforms the other models in both regions, especially in the flank region.
35 Notably, as a time-dependent three-dimensional model, the POS model seldom produces poor predictions, with RMSE exceeding 3 R_{E} in only rare cases.

4.1 Time-dependent feature

The models' prediction accuracies are listed in Table 3; it
40 can be seen that all evaluated models exhibit remarkable predictive capabilities, with $\Delta < 1 R_{\text{E}}$, aligning closely with other statistical results found in the literature (Staples et al., 2020b). It should be noted that the Δ values calculated for other models in this study may slightly differ from those re-
45 ported in their original papers. This discrepancy arises due to our use of a significantly larger MCE dataset for comparison.

Notably, the POS model demonstrates superior predictive performance, with an average improvement of 17.9 % over the other models. Additionally, time-independent mod-
50 els have inherent limitations when capturing the dynamic response of the magnetosphere to solar wind fluctuations, particularly when the magnetopause standoff distance is not
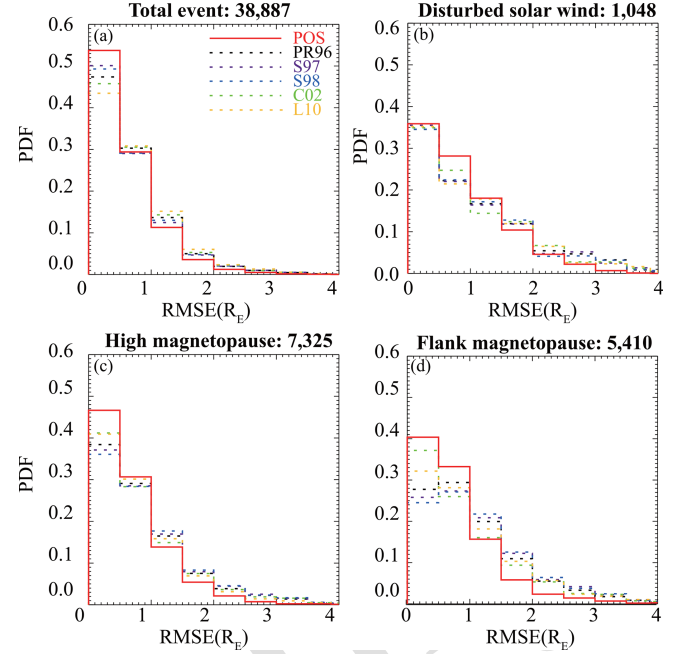
Figure 4. Distribution of models' RMSE in total **(a)** and under disturbed solar wind conditions **(b)**; **(c)** and **(d)** show the prediction accuracies for the higher-latitude magnetopause region ($|\theta| \geq 30°$) and the magnetopause flank region ($|\varphi| \geq 60°$), respectively.

Table 3. Prediction accuracies of the five models and the POS for all MCEs and for MCEs under disturbed solar wind conditions.

Model name	Total (38 887 MCEs)		$[\sigma(P_{\text{dyn}})/< P_{\text{dyn}} >]$ > 100 % (1048 MCEs)	
	$\Delta(R_{\text{E}})$	$\delta(\Delta)/\Delta_{\text{POS}}$	$\Delta(R_{\text{E}})$	$\delta(\Delta)/\Delta_{\text{POS}}$
PR96	0.899	+16.1 %	1.389	+23.6 %
S97	0.884	+14.2 %	1.383	+23.0 %
S98	0.894	+15.5 %	1.388	+23.5 %
C02	0.926	+19.6 %	1.325	+17.9 %
L10	0.960	+24.0 %	1.377	+22.5 %
POS	0.774	Average: 17.9 %	1.124	Average: 22.1 %

in phase with the P_{dyn} (Archer et al., 2019). In cases of highly disturbed upstream solar wind conditions, where the ratio of the standard deviation of P_{dyn} to the average P_{dyn}
55 ($\sigma(P_{\text{dyn}})/< P_{\text{dyn}} >$) exceeds 100 %, the POS model shows an even greater improvement in predictive accuracy, with a 22.1 % enhancement compared to other models. These results suggest that by incorporating time-dependent effects into magnetopause modelling, particularly during periods
60 of solar wind disturbance, the POS model can more effectively capture the non-linear and out-of-phase responses of the magnetopause to rapidly changing solar wind conditions. These results also indicate that the time-dependent model represents an obvious advancement in predicting and under-
65 standing magnetospheric dynamics across a wide range of solar wind conditions.

The magnetopause is rarely static, exhibiting continuous motion under varying solar wind conditions and displaying complex dynamics during both intense disturbances and gentle changes. A notable feature of these dynamics is the periodic oscillation within the Pc5 frequency range (2–7 mHz), often termed the "magic frequency" in magnetospheric physics (Samson et al., 1992; Plaschke et al., 2009a, b). The magnetopause oscillations can be driven by quasi-periodic solar wind dynamic fluctuations or explained by magnetospheric cavity mode and Kruskal–Schwarzschild mode (Archer et al., 2013; Kruskal and Schwarzschild, 1954; Kepko and Spence, 2003; Kivelson et al., 1984). Our previous research indicates that the oscillations of the magnetopause ought to have eigenfrequencies (f_0) which are determined by the restoring force (P_B), the external driving force (P_{dyn}), and the damping force (P_{damp}) (Halliday et al., 2021; Freeman et al., 1995; Gu et al., 2023). The magnetopause will respond to solar wind conditions with phase differences ranging from 0 to 180°, depending on the driving frequency of the solar wind (f_{drive}). The magnetopause behaves as a low-pass filter, effectively screening out very high-frequency solar wind fluctuations (e.g. $f_{drive} > 15 f_0$, where f_0 is the eigenfrequency of the magnetopause). This filtering effect results in smoother predictions of magnetopause behaviour, which can be found in Fig. 5. For relatively high fluctuations (e.g. $15 f_0 > f_{drive} > 2 f_0$), the phase difference between the solar wind and the magnetopause approaches 180°, indicating an anti-phase response. At resonance ($f_{drive} \approx f_0$), the magnetopause exhibits a 90° phase lag relative to the solar wind forcing. Conversely, the magnetopause only behaves in-phase with the solar wind under low-frequency fluctuations ($f_{drive} < 0.5 f_0$), which is the scenario typically revealed by time-independent models.

The time-dependent POS model demonstrates the capability to depict these magnetospheric oscillations and the phase differences accurately. Figure 5 presents two specific cases illustrating the POS model's time-dependent performances compared with subsolar MCEs projected from THEMIS. In Case I, both models initially predict the magnetopause position at $\sim 11.5\,R_E$ before a pressure pulse in the solar wind. The POS model uniquely predicts four oscillations around its equilibrium position ($\sim 10\,R_E$) before the magnetopause reaches a new pressure balance. This dynamic behaviour cannot be physically captured by any time-independent models. In Case II, the POS model accurately captures the oscillations around 21:24–21:33 UT, which are not all in-phase with the solar wind dynamic pressure (P_{dyn}). Notably, the POS model depicts anti-phase responses observed in the second and third crossings, while the S98 model shows a reverse trend in motion, which deviates more from the observations. These results suggest that by incorporating time-dependent effects into magnetopause modelling, particularly during periods of solar wind disturbance, the POS model can more effectively capture the non-linear and out-of-phase responses
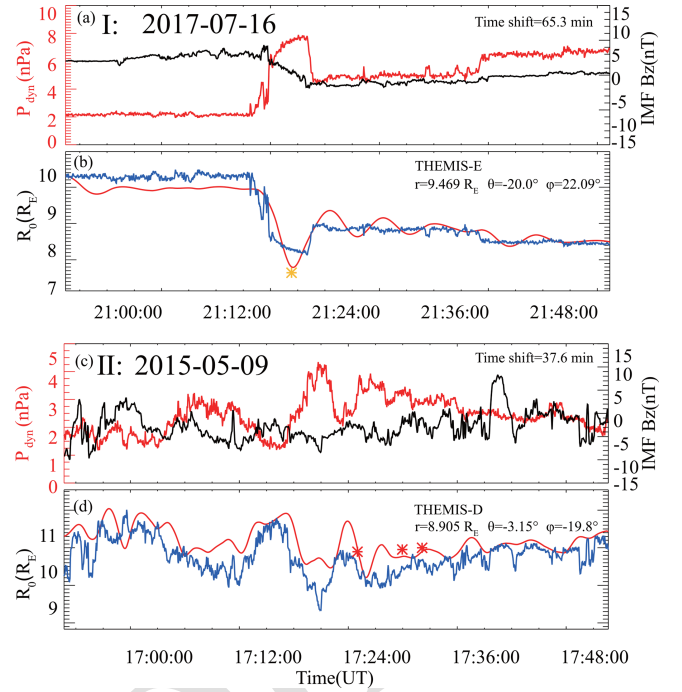
Figure 5. Case study of the overall oscillation of the magnetopause using the time-independent model S98 and the time-dependent POS model to predict its position. Panels **(a)** and **(c)** show the corresponding upstream solar wind dynamic pressure P_{dyn} (red line) and the interplanetary magnetic field B_z component (black line) observed by WIND with time shifts of 65.3 and 37.6 min, respectively. Panels **(b)** and **(d)** show the predictions of the S98 (blue) and the POS (red) models based on the solar wind input; the asterisks represent the subsolar positions of MCEs projected from THEMIS.

of the magnetopause to rapidly changing solar wind conditions.

4.2 Three-dimensional characteristic

The POS model developed here incorporates the asymmetrical effects of dipole tilt angles, latitude, and longitude differences, as integrated into Eqs. (2) and (3). The model's parameters were comprehensively calibrated, allowing it to more accurately depict the three-dimensional shape of the magnetopause. To assess its validity across different magnetopause regions, extensive tests were performed, with results presented in Table 4. In the higher-latitude region of the magnetopause ($|\theta| \geq 30°$), a region where many models face challenges, the POS model, alongside the L10 model, demonstrates superior performance, showing an impressive 27.0 % improvement in accuracy compared to other models. Similarly, in the flank regions ($|\varphi| \geq 60°$), where surface waves and other magnetospheric fluctuations complicate position and shape determination, the POS model maintains its high accuracy, with a 33.3 % improvement over other models. These results suggest that the POS model offers a more

accurate and comprehensive representation of the magnetopause across its entire structure, outperforming other models in both higher-latitude and flank regions.

Surface waves are a distinct feature of the magnetopause, originating from various factors, including the solar wind conditions, bow shock dynamics, and instabilities within the magnetopause and the magnetosphere under specific conditions. Several localized physical processes have been identified as potential drivers of these surface waves, including the Kelvin–Helmholtz instability, magnetic reconnection, and flux transfer events (Hartinger et al., 2013; Agapitov et al., 2009; Archer et al., 2021). It is also found that tailward-moving surface wavelets could be driven by disturbed solar wind conditions (large $\sigma(P_{\mathrm{dyn}})/<P_{\mathrm{dyn}}>$) (Sibeck et al., 1989). Our previous study revealed a distinct mechanism for the formation of surface-wave-like structures in the magnetopause (Gu et al., 2023). The interplay between dynamic pressure (P_{dyn}), magnetic pressure (P_{b}), and damping pressure (P_{damp}) results in different oscillation periods at various points on the magnetopause. These variations create a time lag within the magnetopause structure, manifesting as a surface-wave-like pattern. Figure 6 shows a surface-wave-like structure predicted by the POS model during relatively disturbed upstream solar wind conditions. The POS model's predictions are compared with those of the C02 model, which has been demonstrated as the most effective time-independent model in the flank region according to our evaluation. Figure 6 presents a specific case study illustrating the POS model's time-dependent performance compared with the positions of the THEMIS MCEs mapped to the X–Y plane. Figure 6a displays the solar wind dynamic pressure and the north–south component of the interplanetary magnetic field. The radial positions of the different points in the magnetopause in the X–Y plane ($Z = 0$), as calculated by our model (being fully three-dimensional) exhibiting an asymmetrical flank region, are traced in Fig. 6b. Positive and negative flanks respond differently to variations in the solar wind, with discrepancies becoming more pronounced at higher φ. In this specific example, the dusk region is more significantly disturbed than the dawn region. Notably, the magnetopause shapes calculated in Fig. 6c–e reveal surface-wave-like structures evolving over time. THEMIS MCEs observed in the flank region corroborate this predicted surface-wave-like structure, indicating that the magnetopause position predicted by the POS model is more accurate than the position predicted by the C02 model.

The POS model's predictions are compared with those of the C02 model, which has been demonstrated as the most effective time-independent model in the flank region according to our evaluation. Figure 6 illustrates a surface-wave-like structure predicted by the POS model during relatively disturbed upstream solar wind conditions. The predicted surface-wave-like structure is corroborated by THEMIS MCEs in the flank region, where the actual magnetopause
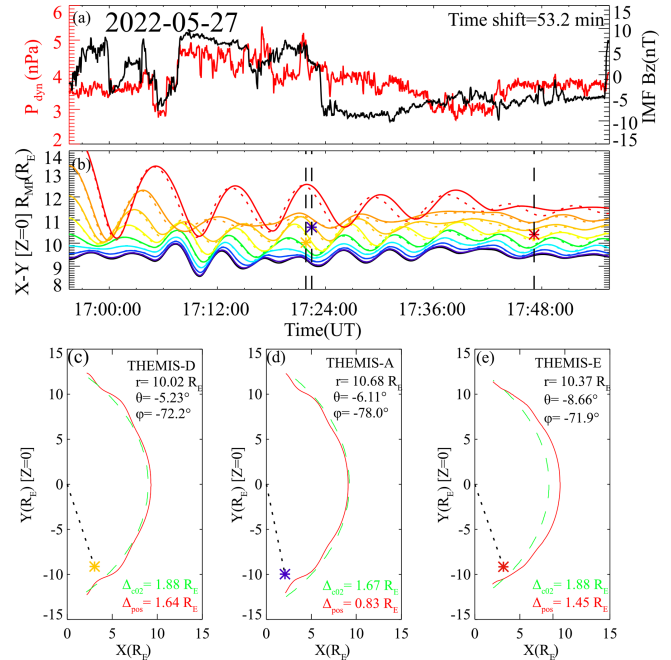
Figure 6. A surface-wave-like structure in the X–Y magnetopause flank region. Panel **(a)** shows the corresponding solar wind dynamic pressure (red) and IMF B_z component (black). Panel **(b)** shows red, orange, light orange, yellow, green, blue, dark blue, purple, and black colours representing the initial magnetopause positions at $\varphi = \pm80, \pm70, \pm60, \pm50, \pm40, \pm30, \pm20, \pm10$, and $0°$, respectively. The dotted line indicates the corresponding negative value of φ. The asterisks in purple (THEMIS-A), yellow (THEMIS-D), and red (THEMIS-E) indicate the satellite observations of MCEs projected onto the X–Y plane. Panels **(c)**, **(d)**, and **(e)** show the shape of the magnetopause in the X–Y plane at different times predicted by the POS model (red dashed line) and the C02 model (green dotted line); the asterisks represent the THEMIS MCE positions mapped to the X–Y plane.

position is closer to Earth than the position predicted by the C02 model.

5 Discussion and conclusions

Accurately calculating the position of the magnetopause is essential for space weather forecasting and understanding the underlying physical mechanisms involved in the solar wind–magnetosphere interaction. In this work, we developed the POS model, the first time-dependent three-dimensional magnetopause model based on quasi-elastodynamic theory. By incorporating key solar wind parameters such as P_{dyn}, IMF B_z, and Φ, this model effectively depicts magnetopause dynamics. The POS model offers a new approach to describing the magnetopause position, overall oscillation, and surface-wave-like structures as interconnected phenomena. Its time-dependent feature excels in capturing dynamic processes, particularly under highly disturbed solar wind conditions.

Table 4. The prediction accuracies of the five models and the POS for higher-latitude and flank regions.

Model name	$|\theta| \geq 30°$ (7325 MCEs)		$|\varphi| \geq 60°$ (5410 MCEs)	
	$< \Delta > (R_E)$	$\delta(\Delta)/\Delta_{POS}$	$\Delta (R_E)$	$\delta(\Delta)/\Delta_{POS}$
PR96	1.149	+27.8%	1.315	+31.8%
S97	1.180	+31.3%	1.388	+39.1%
S98	1.195	+32.9%	1.403	+40.6%
C02	1.130	+25.7%	1.268	+27.1%
L10	1.053	+17.1%	1.278	+28.0%
POS	0.899	Average: 27.0%	0.998	Average: 33.3%

The three-dimensional nature allows for accurate depiction of the overall magnetopause shape, with notable precision in higher-latitude regions and flank areas. This capability addresses limitations in existing models and provides a more comprehensive picture of magnetopause dynamics from a different perspective. However, there are still limitations and areas for improvement that future research should address.

1. *Adaptation to extreme solar wind conditions.* Similar to the force–deformation relationship of a spring, which requires a specific range of applicability, the POS model has not been specifically optimized for extreme solar wind conditions (e.g. $P_{dyn} < 0.5$ nPa and $P_{dyn} > 40$ nPa). When the solar wind dynamic pressure is low, the quasi-elastic process between the solar wind and the magnetopause exhibits stronger damping characteristics, while at very high solar wind dynamic pressures, the magnetopause shows increased rigidity. Future iterations could incorporate more suitable damping coefficients and include P_{dyn} in the magnetospheric compressibility coefficient to broaden the model's applicability range.

2. *Incorporation of additional solar wind factors.* Existing research has shown that even under similar solar wind dynamic pressure conditions, changes in the solar wind density and velocity have distinct effects on magnetopause position (Samsonov et al., 2020). Additionally, the influence of the solar wind temperature, more comprehensive IMF effects (e.g. B_x and B_y), and other solar wind components (e.g. alpha particles) on magnetopause position are not reflected in the current model. Moreover, magnetosheath transient effects and other perturbations on the magnetopause position are not addressed (Silveira et al., 2024; Silveira and Sibeck, 2023; Sibeck et al., 2022). Future models could consider introducing these factors to achieve better predictive results.

3. *Extension of the nightside magnetopause.* The current POS model is primarily based on the dayside quasi-elastodynamic theory and is calibrated and validated using dayside MCEs. In the future, the model's calculation results for the nightside region could be improved by combining the fitting approach of empirical models with a more flexible curve function calibrated using a larger number of nightside MCE observations.

4. *Improved representation of the cusp region.* Accurately modelling the magnetopause cusp region, shaped by Earth's dipole field, remains challenging. While some models approximate this region by fitting two distinct curves, capturing its shape and position precisely is complex. Improving the representation of the cusp region will require further analysis of higher-latitude satellite data to enhance model accuracy.

5. *Fine-tuning of model parameters.* Further refinement of model parameters, potentially through machine learning techniques or implementing piecewise functions for different regions, could improve the model's accuracy. However, as noted in the introduction, it is important to balance model complexity with practicality. Overly complex parameter expressions can lead to increased inconvenience and higher computational costs. For those seeking the highest possible prediction accuracy, a more practical approach might involve using numerical simulations.

The upcoming SMILE mission (Solar Wind Magnetosphere Ionosphere Link Explorer), a joint mission between the Chinese Academy of Sciences and the European Space Agency, is set to launch in 2025 (Branduardi-Raymont et al., 2018; Wang and Branduardi-Raymont, 2018). This mission will provide more detailed data on magnetopause position and polar-cap shape over time, enhancing the ability to validate and refine existing magnetopause models.

In summary, this study introduces the POS model, the first time-dependent three-dimensional magnetopause model based on quasi-elastodynamic theory. Unlike time-independent models, the POS model effectively captures the dynamic movement of the magnetopause under varying solar wind conditions. When compared to five widely used models, the POS model demonstrates superior predictive accuracy, showing a 17.9% improvement with RMSE = 0.774 R_E. As a time-dependent model, it demonstrated superior accuracy under highly disturbed solar wind conditions (22.1%

better). Its three-dimensional nature allows for enhanced accuracy in higher-latitude regions (27.0 % better) and flank regions (33.3 % better) of the magnetopause. Moreover, compared to numerical simulations, the POS model offers a concise formulation with rapid computational speed, making it feasible for direct deployment on satellites in the future – when onboard chips could complete calculations – greatly enhancing satellite intelligence. By providing a more precise and dynamic representation of the magnetopause, the POS model enhances our ability to predict and analyse space weather events and may also offer new insights and methodologies for developing magnetopause models for other planets.

Code and data availability. The current version of the model is available at the Space Weather Committee of the Chinese Geophysical Society website-POS model page (http://www.spaceweather.org.cn/pos_model, last access: 24 June 2025; Gu et al., 2023). For reproducibility, the exact version of the model code used to produce the results in this paper, along with the list of MCEs, is permanently archived on Zenodo at https://doi.org/10.5281/zenodo.15162611 (Wang, 2025). The THEMIS Level 2 data products used in this study are publicly available through the NASA Coordinated Data Analysis Web (CDAWeb) (https://cdaweb.gsfc.nasa.gov/pub/data/themis/, last access: 24 June 2025; Angelopoulos, 2008) and the CLUSTER Level 2 data products are also available from CDAWeb (https://cdaweb.gsfc.nasa.gov/pub/data/cluster/, last access: 24 June 2025; Escoubet et al., 2001). The Wind spacecraft's data are also available from NASA CDAWeb (https://cdaweb.gsfc.nasa.gov/pub/data/wind/, last access: 24 June 2025; Lin et al., 1995).

Author contributions. YW designed the model. YXG developed the model code and carried it out. YXG and YW prepared the original manuscript. YXG and XJS prepared the MCE list. FSW, XSF, AS, XJS, BYW, PBZ, CWJ, YLC, XJX, and ZLZ discussed the scientific results and reviewed and revised the paper.

Competing interests. The contact author has declared that none of the authors have any competing interests.

Acknowledgements. We thank NASA, the Goddard Space Flight Center (GSFC), and the CDAWeb data facility for providing the Wind, THEMIS, and CLUSTER data.

Financial support. This work was jointly supported by the National Key R&D Program of China (grant no. 2022YFF0503900), the National Natural Science Foundation of China (grant. nos. 42174199 and 42030204), the China Scholarship Council (grant no. 202306120305), the Specialized Research Fund for State Key Laboratory of Solar Activity and Space Weather, the Guangdong Basic and Applied Basic Research Foundation (grant no. 2023B1515040021), the Shenzhen Technology Project (grant nos. JCYJ20210324121210027, RCJC20210609104422048, and GXWD20220817152453003), and the Shenzhen Key Laboratory Launching Project (grant no. ZDSYS20210702140800001).

Review statement. This paper was edited by Tatiana Egorova and reviewed by two anonymous referees.

References

Agapitov, O., Glassmeier, K.-H., Plaschke, F., Auster, H.-U., Constantinescu, D., Angelopoulos, V., Magnes, W., Nakamura, R., Carlson, C. W., Frey, S., and McFadden, J. P.: Surface waves and field line resonances: A THEMIS case study, J. Geophys. Res.-Space, 114, A00C27, https://doi.org/10.1029/2008ja013553, 2009.

Ala-Lahti, M., Pulkkinen, T. I., Pfau-Kempf, Y., Grandin, M., and Palmroth, M.: Energy Flux Through the Magnetopause During Flux Transfer Events in Hybrid-Vlasov 2D Simulations, Geophys. Res. Lett., 49, e2022GL100079, https://doi.org/10.1029/2022gl100079, 2022.

Anderson, K. A., Binsack, J. H., and Fairfield, D. H.: Hydromagnetic disturbances of 3- to 15-minute period on magnetopause and their relation to bow shock spikes, J. Geophys. Res., 73, 2371–2386, https://doi.org/10.1029/JA073i007p02371, 1968.

Angelopoulos, V.: The THEMIS mission, Space Sci. Rev., 141, 5–34, https://doi.org/10.1007/s11214-008-9336-1, 2008.

Archer, M. O., Hartinger, M. D., and Horbury, T. S.: Magnetospheric "magic" frequencies as magnetopause surface eigenmodes, Nat. Commun., 40, 5003–5008, https://doi.org/10.1002/grl.50979, 2013.

Archer, M. O., Hartinger, M. D., Plaschke, F., Southwood, D. J., and Rastaetter, L.: Magnetopause ripples going against the flow form azimuthally stationary surface waves, Nat. Commun., 12, 5697, https://doi.org/10.1038/s41467-021-25923-7, 2021.

Archer, M. O., Hietala, H., Hartinger, M. D., Plaschke, F., and Angelopoulos, V.: Direct observations of a surface eigenmode of the dayside magnetopause, Nat. Commun., 10, 615, https://doi.org/10.1038/s41467-018-08134-5, 2019.

Ashida, Y., Yamakawa, H., Funaki, I., Usui, H., Kajimura, Y., and Kojima, H.: Thrust Evaluation of Small-Scale Magnetic Sail Spacecraft by Three-Dimensional Particle-in-Cell Simulation, J. Propul. Power, 30, 186–196, https://doi.org/10.2514/1.B35026, 2014.

Aubry, M. P., Russell, C. T., and Kivelson, M. G.: Inward motion of the magnetopause before a substorm, J. Geophys. Res., 75, 7018–7031, 1970.

Auster, H. U., Glassmeier, K. H., Magnes, W., Aydogar, O., Baumjohann, W., Constantinescu, D., Fischer, D., Fornacon, K. H., Georgescu, E., Harvey, P., Hillenmaier, O., Kroth, R., Lud-

lam, M., Narita, Y., Nakamura, R., Okrafka, K., Plaschke, F., Richter, I., Schwarzl, H., Stoll, B., Valavanoglou, A., and Wiedemann, M.: The THEMIS Fluxgate Magnetometer, Space Sci. Rev., 141, 235–264, https://doi.org/10.1007/s11214-008-9365-9, 2008.

Balogh, A., Dunlop, M. W., Cowley, S. W. H., Southwood, D. J., Thomlinson, J. G., Glassmeier, K. H., Musmann, G., Lühr, H., Buchert, S., Acuña, M. H., Fairfield, D. H., Slavin, J. A., Riedler, W., Schwingenschuh, K., and Kivelson, M. G.: The Cluster Magnetic Field Investigation, in: The Cluster and Phoenix Missions, edited by: Escoubet, C. P., Russell, C. T., and Schmidt, R., Springer Netherlands, Dordrecht, 65–91, https://doi.org/10.1007/978-94-011-5666-0_3, 1997.

Beard, D. B.: The interaction of the terrestrial magnetic field with the solar corpuscular radiation, J. Geophys. Res., 65, 3559–3568, https://doi.org/10.1029/JZ065i011p03559, 1960.

Boardsen, S. A., Eastman, T. E., Sotirelis, T., and Green, J. L.: An empirical model of the high-latitude magnetopause, J. Geophys. Res.-Space., 105, 23193–23219, https://doi.org/10.1029/1998JA000143, 2000.

Borovsky, J. E. and Alejandro Valdivia, J.: The Earth's Magnetosphere: A Systems Science Overview and Assessment, Surv. Geophys., 39, 817–859, https://doi.org/10.1007/s10712-018-9487-x, 2018.

Børve, S., Sato, H., Pécseli, H., and Trulsen, J.: Minute-scale period oscillations of the magnetosphere, Ann. Geophys., 29, 663–671, https://doi.org/10.5194/angeo-29-663-2011, 2011.

Branduardi-Raymont, G., Wang, C., Escoubet, C. P., Adamovic, M., Agnolon, D., Berthomier, M., Carter, J. A., Chen, W., Colangeli, L., Collier, M., Connor, H. K., Dai, L., Dimmock, A., Djazovski, O., Donovan, E., Eastwood, J. P., Enno, G., Giannini, F., Huang, L., Kataria, D., Kuntz, K., Laakso, H., Li, J., Li, L., Lui, T., Loicq, J., Masson, A., Manuel, J., Parmar, A., Piekutowski, T., Read, A. M., Samsonov, A., Sembay, S., Raab, W., Ruciman, C., Shi, J. K., Sibeck, D. G., Spanswick, E. L., Sun, T., Symonds, K., Tong, J., Walsh, B., Wei, F., Zhao, D., Zheng, J., Zhu, X., and Zhu, Z.: SMILE Definition Study Report (Red Book), European Space Agency, ESA/SCI(1), 1–86, https://doi.org/10.5270/esa.smile.definition_study_report-2018-12, 2018.

Chao, J. K., Wu, D., Lin, C. H., Yang, Y. H., Wang, X. Y., Kessel, M., Chen, S. H., and Lepping, R. P.: Models for the size and shape of the Earth's magnetopause and bow shock, COSPAR Coll., 12, 127–135, https://doi.org/10.1016/S0964-2749(02)80212-8, 2002.

Chapman, S. and Ferraro, V. C. A.: A New Theory of Magnetic Storms, J. Geophys. Res., 38, 79–96, https://doi.org/10.1038/126129a0, 1930.

Chen, C. X. and Wolf, R. A.: Theory of thin-filament motion in Earth's magnetotail and its application to bursty bulk flows, J. Geophys. Res.-Space, 104, 14613–14626, https://doi.org/10.1029/1999ja900005, 1999.

Chen, Y.-W., Shue, J.-H., Zhong, J., and Shen, H.-W.: Anomalous Response of Mercury's Magnetosphere to Solar Wind Compression: Comparison to Earth, Astrophys. J., 957, 26, https://doi.org/10.3847/1538-4357/acf655, 2023.

Choe, J. Y. and Beard, D. B.: The compressed geomagnetic field as a function of dipole tilt, Planet. Space Sci., 22, 595–608, https://doi.org/10.1016/0032-0633(74)90093-2, 1974a.

Choe, J. Y. and Beard, D. B.: The near earth magnetic field of the magnetotail current, Planet. Space Sci., 22, 609–615, https://doi.org/10.1016/0032-0633(74)90094-4, 1974b.

Collado-Vega, Y. M., Dredger, P., Lopez, R. E., Khurana, S., Rastaetter, L., Sibeck, D., and Anastopulos, M.: Magnetopause Standoff Position Changes and Geosynchronous Orbit Crossings: Models and Observations, Space Weather, 21, e2022SW003212, https://doi.org/10.1029/2022SW003212, 2023.

Halliday, D., Resnick, R., and Walker, J.: Fundamentals of Physics, Extended, 12th Edition, in: Fundamentals of Physics, Extended, 12th Edn., Wiley, 456–458, ISBN 978-1-119-77351, 2021.

Desai, R. T., Freeman, M. P., Eastwood, J. P., Eggington, J. W. B., Archer, M. O., Shprits, Y. Y., Meredith, N. P., Staples, F. A., Rae, I. J., Hietala, H., Mejnertsen, L., Chittenden, J. P., and Horne, R. B.: Interplanetary Shock–Induced Magnetopause Motion: Comparison Between Theory and Global Magnetohydrodynamic Simulations, Geophys. Res. Lett., 48, e2021GL092554, https://doi.org/10.1029/2021gl092554, 2021.

Dungey, J. W.: Interplanetary Magnetic Field and the Auroral Zones, Phys. Rev. Lett., 6, 47–48, https://doi.org/10.1103/PhysRevLett.6.47, 1961.

Eastwood, J. P., Hietala, H., Toth, G., Phan, T. D., and Fujimoto, M.: What Controls the Structure and Dynamics of Earth's Magnetosphere?, Space Sci. Rev., 188, 251–286, https://doi.org/10.1007/s11214-014-0050-x, 2015.

Escoubet, C. P., Fehringer, M., and Goldstein, M.: Introduction The Cluster mission, Ann. Geophys., 19, 1197–1200, https://doi.org/10.5194/angeo-19-1197-2001, 2001.

Fairfield, D. H.: Average and unusual locations of the Earth's magnetopause and bow shock, J. Geophys. Res., 76, 6700–6716, https://doi.org/10.1029/JA076i028p06700, 1971.

Feng, X.: Current Status of MHD Simulations for Space Weather, in: Magnetohydrodynamic Modeling of the Solar Corona and Heliosphere, edited by: Feng, X., Springer Singapore, Singapore, 1–123, https://doi.org/10.1007/978-981-13-9081-4_1, 2020.

Ferraro, V. C. A.: On the theory of the first phase of a geomagnetic storm: A new illustrative calculation based on an idealised (plane not cylindrical) model field distribution, J. Geophys. Res., 57, 15–49, https://doi.org/10.1029/JZ057i001p00015, 1952.

Formisano, V., Domingo, V., and Wenzel, K.-P.: The three-dimensional shape of the magnetopause, Planet. Space Sci., 27, 1137–1149, https://doi.org/10.1016/0032-0633(79)90134-x, 1979.

Freeman, M. P. and Farrugia, C. J.: Magnetopause motions in a Newton-Busemann approach, Natl. Adv. Sci. I. C.-Mat., 509, 15–26, 1998.

Freeman, M. P., Freeman, N. C., and Farrugia, C. J.: A Linear Perturbation Analysis of Magnetopause Motion in the Newton-Busemann Limit, Ann. Geophys., 13, 907–918, https://doi.org/10.1007/s005850050230, 1995.

Gargaté, L., Fonseca, R. A., Bingham, R., and Silva, L. O.: Expansion of a plasma cloud into the solar wind, IEEE T. Plasma Sci., 36, 1168–1169, https://doi.org/10.1109/tps.2008.922424, 2008.

Grimmich, N., Plaschke, F., Grison, B., Prencipe, F., Escoubet, C. P., Archer, M. O., and Maggiolo, R: Cluster Magnetopause Crossings between 2001 and 2020, OSF Home [data set], https://doi.org/10.17605/OSF.IO/PXCTG, 2024.

Gu, Y. X., Wang, Y., Wei, F. S., Feng, X. S., Song, X. J., Wang, B. Y., Zuo, P. B., Jiang, C. W., Xu, X. J., and Zhou, Z. L.: Quasi-elastodynamic Processes Involved in the Interaction between Solar Wind and Magnetosphere, Astrophys. J., 946, 102, https://doi.org/10.3847/1538-4357/acbe9b, 2023.

Haerendel, G.: Field-Aligned Currents in the Earth's Magnetosphere, in: Physics of Magnetic Flux Ropes, Geophys. Monogr. Ser., 539–553, https://doi.org/10.1029/GM058p0539, 1990.

Hartinger, M. D., Turner, D. L., Plaschke, F., Angelopoulos, V., and Singer, H.: The role of transient ion foreshock phenomena in driving Pc5 ULF wave activity, J. Geophys. Res.-Space, 118, 299–312, https://doi.org/10.1029/2012JA018349, 2013.

Hu, Y.-Q., Guo, X.-C., Li, G.-Q., Wang, C., and Huang, Z.-H.: Oscillation of Quasi-Steady Earth's Magnetosphere, Chinese Physics Letters, 22, 2723, https://doi.org/10.1088/0256-307x/22/10/073, 2005.

Kepko, L. and Spence, H. E.: Observations of discrete, global magnetospheric oscillations directly driven by solar wind density variations, J. Geophys. Res.-Space, 108, 1257, https://doi.org/10.1029/2002ja009676, 2003.

Kivelson, M. G., Etcheto, J., and Trotignon, J. G.: Global compressional oscillations of the terrestrial magnetosphere: The evidence and a model, J. Geophys. Res.-Space, 89, 9851–9856, https://doi.org/10.1029/JA089iA11p09851, 1984.

Kruskal, M. and Schwarzschild, M.: Some instabilities of a completely ionized plasma, P. Roy. Soc. Lond. Ser. A-Math., 223, 348–360, https://doi.org/10.1098/rspa.1954.0120, 1954.

Lepping, R. P., Acuna, M. H., Burlaga, L. F., Farrell, W. M., Slavin, J. A., Schatten, K. H., Mariani, F., Ness, N. F., Neubauer, F. M., Whang, Y. C., Byrnes, J. B., Kennon, R. S., Panetta, P. V., Scheifele, J., and Worley, E. M.: The WIND magnetic field investigation, Space Sci. Rev., 71, 207–229, https://doi.org/10.1007/BF00751330, 1995.

Lin, R. P., Anderson, K. A., Ashford, S., Carlson, C., Curtis, D., Ergun, R., Larson, D., McFadden, J., McCarthy, M., Parks, G. K., Rème, H., Bosqued, J. M., Coutelier, J., Cotin, F., D'Uston, C., Wenzel, K. P., Sanderson, T. R., Henrion, J., Ronnet, J. C., and Paschmann, G.: A three-dimensional plasma and energetic particle investigation for the Wind spacecraft, Space Sci. Rev., 71, 125–153, 1995.

Lin, R. L., Zhang, X. X., Liu, S. Q., Wang, Y. L., and Gong, J. C.: A three-dimensional asymmetric magnetopause model, J. Geophys. Res.-Space, 115, A04207, https://doi.org/10.1029/2009JA014235, 2010.

Lyon, J. G., Fedder, J. A., and Mobarry, C. M.: The Lyon-Fedder-Mobarry (LFM) global MHD magnetospheric simulation code, J. Atmos. Sol.-Terr. Phys., 66, 1333–1350, https://doi.org/10.1016/j.jastp.2004.03.020, 2004.

Mann, I. R., Murphy, K. R., Ozeke, L. G., Rae, I. J., Milling, D. K., Kale, A. A., and Honary, F. F.: The Role of Ultralow Frequency Waves in Radiation Belt Dynamics, in: Dynamics of the Earth's Radiation Belts and Inner Magnetosphere, 69–92, https://doi.org/10.1029/2012GM001349, 2012.

Matsuoka, H., Takahashi, K., and Yumoto, K.: Observation and modeling of compressional Pi 3 magnetic pulsations, J. Geophys. Res.-Space, 100, 12103–12115, https://doi.org/10.1029/94JA03668, 1995.

McFadden, J., Carlson, C., Larson, D., Ludlam, M., Abiad, R., Elliott, B., Turin, P., Marckwordt, M., and Angelopoulos, V.: The THEMIS ESA plasma instrument and in-flight calibration, Space Sci. Rev., 141, 277–302, https://doi.org/10.1007/s11214-008-9440-2, 2008.

Mead, G. D. and Beard, D. B.: Shape of the geomagnetic field solar wind boundary, J. Geophys. Res., 69, 1169–1179, https://doi.org/10.1029/jz069i007p01169, 1964.

Merkin, V. G. and Lyon, J. G.: Effects of the low-latitude ionospheric boundary condition on the global magnetosphere, J. Geophys. Res.-Space, 115, A10202, https://doi.org/10.1029/2010JA015461, 2010.

Moritaka, T., Kajimura, Y., Usui, H., Matsumoto, M., Matsui, T., and Shinohara, I.: Momentum transfer of solar wind plasma in a kinetic scale magnetosphere, Phys. Plasmas, 19, https://doi.org/10.1063/1.3683560, 2012.

Mottez, F.: Relationship between Alfvén Wave and Quasi-Static Acceleration in Earth's Auroral Zone, in: Low-Frequency Waves in Space Plasmas, 121–138, https://doi.org/10.1002/9781119055006.ch8, 2016.

Olson, W. P.: The shape of the tilted magnetopause, J. Geophys. Res.-Space, 74, 5642–5651, https://doi.org/10.1029/JA074i024p05642, 1969.

Omelchenko, Y. A., Roytershteyn, V., Chen, L. J., Ng, J., and Hietala, H.: HYPERS simulations of solar wind interactions with the Earth's magnetosphere and the Moon, J. Atmos. Sol.-Terr. Phys., 215, 105581, https://doi.org/10.1016/j.jastp.2021.105581, 2021.

Petrinec, S. M.: Nowcasting and Forecasting the Magnetopause and Bow Shock Locations Based on Empirical Models and Real-Time Solar Wind Data, in: Space Weather, Geophysical Monograph Series, 257–263, https://doi.org/10.1029/GM125p0257, 2001.

Petrinec, S. M. and Russell, C. T.: Near-Earth magnetotail shape and size as determined from the magnetopause flaring angle, J. Geophys. Res.-Space, 101, 137–152, https://doi.org/10.1029/95JA02834, 1996.

Plaschke, F.: ULF Waves at the Magnetopause, in: Low-Frequency Waves in Space Plasmas, Geophysical Monograph Series, 193–212, https://doi.org/10.1002/9781119055006.ch12, 2016.

Plaschke, F., Glassmeier, K.-H., Sibeck, D. G., Auster, H. U., Constantinescu, O. D., Angelopoulos, V., and Magnes, W.: Magnetopause surface oscillation frequencies at different solar wind conditions, Ann. Geophys., 27, 4521–4532, https://doi.org/10.5194/angeo-27-4521-2009, 2009a.

Plaschke, F., Glassmeier, K.-H., Auster, H. U., Constantinescu, O. D., Magnes, W., Angelopoulos, V., Sibeck, D. G., and McFadden, J. P.: Standing Alfvén waves at the magnetopause, Geophys. Res. Lett., 36, L02104, https://doi.org/10.1029/2008GL036411, 2009b.

Powell, K. G., Roe, P. L., Linde, T. J., Gombosi, T. I., and De Zeeuw, D. L.: A solution-adaptive upwind scheme for ideal magnetohydrodynamics, J. Computat. Phys., 154, 284–309, https://doi.org/10.1006/jcph.1999.6299, 1999.

Raeder, J., McPherron, R. L., Frank, L. A., Kokubun, S., Lu, G., Mukai, T., Paterson, W. R., Sigwarth, J. B., Singer, H. J., and Slavin, J. A.: Global simulation of the Geospace Environment Modeling substorm challenge event, J. Geophys. Res.-Space, 106, 381–395, https://doi.org/10.1029/2000JA000605, 2001.

Rème, H., Bosqued, J. M., Sauvaud, J. A., Cros, A., Dandouras, J., Aoustin, C., Bouyssou, J., Camus, T., Cuvilo, J., Martz, C.,

MÉDale, J. L., Perrier, H., Romefort, D., Rouzaud, J., D'Uston, C., MÖBius, E., Crocker, K., Granoff, M., Kistler, L. M., Popecki, M., Hovestadt, D., Klecker, B., Paschmann, G., Scholer, M., Carlson, C. W., Curtis, D. W., Lin, R. P., McFadden, J. P., Formisano, V., Amata, E., Bavassano-Cattaneo, M. B., Baldetti, P., Belluci, G., Bruno, R., Chionchio, G., Di Lellis, A., Shelley, E. G., Ghielmetti, A. G., Lennartsson, W., Korth, A., Rosenbauer, H., Lundin, R., Olsen, S., Parks, G. K., McCarthy, M., and Balsiger, H.: THE CLUSTER ION SPECTROMETRY (CIS) EXPERIMENT, Space Sci. Rev., 79, 303–350, https://doi.org/10.1023/A:1004929816409, 1997.

Russell, C. T.: The structure of the magnetopause, Planet. Space Sci., 51, 731–744, https://doi.org/10.1016/s0032-0633(03)00110-7, 2003.

Samson, J. C., Harrold, B. G., Ruohoniemi, J. M., Greenwald, R. A., and Walker, A. D. M.: Field line resonances associated with mhd wave-guides in the magnetosphere, Geophys. Res. Lett., 19, 441–444, https://doi.org/10.1029/92gl00116, 1992.

Samsonov, A. A., Bogdanova, Y. V., Branduardi-Raymont, G., Sibeck, D. G., and Toth, G.: Is the Relation Between the Solar Wind Dynamic Pressure and the Magnetopause Standoff Distance so Straightforward?, Geophys. Res. Lett., 47, e2019GL086474, https://doi.org/10.1029/2019GL086474, 2020.

Samsonov, A. A., Gordeev, E., Tsyganenko, N. A., Šafránková, J., Němeček, Z., Šimůnek, J., Sibeck, D. G., Tóth, G., Merkin, V. G., and Raeder, J.: Do we know the actual magnetopause position for typical solar wind conditions?, J. Geophys. Res.-Space, 121, 6493–6508, https://doi.org/10.1002/2016JA022471, 2016.

Sato, H., Pécseli, H., Trulsen, J., Sandholt, P. E., and Farrugia, C.: Impulse-driven oscillations of the near-Earth's magnetosphere, Ann. Geophys., 40, 641–663, https://doi.org/10.5194/angeo-40-641-2022, 2022.

Schield, M. A.: Pressure balance between solar wind and magnetosphere, J. Geophys. Res., 74, 1275–1286, https://doi.org/10.1029/JA074i005p01275, 1969.

Shue, J.-H., Song, P., Russell, C. T., Steinberg, J. T., Chao, J. K., Zastenker, G., Vaisberg, O. L., Kokubun, S., Singer, H. J., Detman, T. R., and Kawano, H.: Magnetopause location under extreme solar wind conditions, J. Geophys. Res.-Space, 103, 17691–17700, https://doi.org/10.1029/98JA01103, 1998.

Shue, J. H., Chao, J. K., Fu, H. C., Russell, C. T., Song, P., Khurana, K. K., and Singer, H. J.: A New Functional form to Study the Solar Wind Control of the Magnetopause Size and Shape, J. Geophys. Res., 102, 9497, https://doi.org/10.1029/97ja00196, 1997.

Shue, J. H., Chen, Y. S., Hsieh, W. C., Nowada, M., Lee, B. S., Song, P., Russell, C. T., Angelopoulos, V., Glassmeier, K. H., McFadden, J. P., and Larson, D.: Uneven compression levels of Earth's magnetic fields by shocked solar wind, J. Geophys. Res.-Space, 116, A02203, https://doi.org/10.1029/2010ja016149, 2011.

Sibeck, D. G.: The Magnetospheric and Ionospheric Response to Solar Wind Dynamic Pressure Variations, in: Modeling Magnetospheric Plasma Processes, Geophysical Monograph Series, 1–8, https://doi.org/10.1029/GM062p0001, 1991.

Sibeck, D. G., Silveira, M. V. D., and Collier, M. R.: Tracking the Subsolar Bow Shock and Magnetopause, J. Geophys. Res.-Space, 127, e2022JA030704, https://doi.org/10.1029/2022JA030704, 2022.

Sibeck, D. G., Baumjohann, W., Elphic, R. C., Fairfield, D. H., Fennell, J. F., Gail, W. B., Lanzerotti, L. J., Lopez, R. E., Luehr, H., Lui, A. T. Y., Maclennan, C. G., McEpntire, R. W., Potemra, T. A., Rosenberg, T. J., and Takahashi, K.: The Magnetospheric Response to 8-Minute Period Strong-Amplitude Upstream Pressure Variations, J. Geophys. Res.-Space Physics, 94, 2505–2519, https://doi.org/10.1029/JA094iA03p02505, 1989.

Silveira, M. V. D. and Sibeck, D. G.: A Linear Velocity Gradient in the Subsolar Magnetosheath, J. Geophys. Res.-Space, 128, e2023JA031362, https://doi.org/10.1029/2023JA031362, 2023.

Silveira, M. V. D., Sibeck, D. G., Cardoso, F. R., and Gjerloev, J. W.: Tracking the Subsolar Bow Shock and Magnetopause: Applying the Magnetosheath Velocity Gradient Method, J. Geophys. Res.-Space, 129, e2023JA032166, https://doi.org/10.1029/2023JA032166, 2024.

Smit, G. R.: Oscillatory motion of the nose region of the magnetopause, J. Geophys. Res., 73, 4990–4993, https://doi.org/10.1029/JA073i015p04990, 1968.

Song, P., Elphic, R. C., and Russell, C. T.: ISEE-1 and ISEE-2 observations of the oscillating magnetopause, Geophys. Res. Lett., 15, 744–747, https://doi.org/10.1029/GL015i008p00744, 1988.

Song, P., Sonnerup, B. U. Ö., and Thomsen, M. F. (Eds.): Physics of the Magnetopause, American Geophysical Union, 5260, 364 pp., https://doi.org/10.1126/science.272.5260.364.a, 1996.

Song, X., Zuo, P., and Zhou, Z.: Automatic Identification of Magnetopause Crossing Events, Chinese J. Space Sci., 41, 375–383, https://doi.org/10.3724/SP.J.0254-6124.2021.0303, 2021.

Spreiter, J. R., Summers, A. L., and Alksne, A. Y.: Hydromagnetic flow around the magnetosphere, Planet. Space Sci., 14, 223–253, https://doi.org/10.1016/0032-0633(66)90124-3, 1966.

Staples, F. A., Ashley, R. A., Forsyth, S. C., Jonathan, I., and Rae: THEMIS Magnetopause Crossing Database (1)m, Zenodo [data set], https://doi.org/10.5281/zenodo.3700504, 2020a.

Staples, F. A., Rae, I. J., Forsyth, C., Smith, A. R. A., Murphy, K. R., Raymer, K. M., Plaschke, F., Case, N. A., Rodger, C. J., Wild, J. A., Milan, S. E., and Imber, S. M.: Do Statistical Models Capture the Dynamics of the Magnetopause During Sudden Magnetospheric Compressions?, J. Geophys. Res.-Space, 125, e2019JA027289, https://doi.org/10.1029/2019ja027289, 2020b.

Tóth, G., Sokolov, I. V., Gombosi, T. I., Chesney, D. R., Clauer, C. R., De Zeeuw, D. L., Hansen, K. C., Kane, K. J., Manchester, W. B., Oehmke, R. C., Powell, K. G., Ridley, A. J., Roussev, I. I., Stout, Q. F., Volberg, O., Wolf, R. A., Sazykin, S., Chan, A., Yu, B., and Kóta, J.: Space Weather Modeling Framework: A new tool for the space science community, J. Geophys. Res.-Space, 110, A12226, https://doi.org/10.1029/2005JA011126, 2005.

Tsyganenko, N. A.: A magnetospheric magnetic field model with a warped tail current sheet, Planet. Space Sci., 37, 5–20, https://doi.org/10.1016/0032-0633(89)90066-4, 1989.

Tsyganenko, N. A. and Stern, D. P.: Modeling the global magnetic field of the large-scale Birkeland current systems, J. Geophys. Res.-Space, 101, 27187–27198, https://doi.org/10.1029/96JA02735, 1996.

Tsyganenko, N. A.: Empirical Magnetic Field Models for the Space Weather Program, in: Space Weather, Geophysical Monograph Series, 273–280, https://doi.org/10.1029/GM125p0273, 2001.

Walker, R. J., Lapenta, G., Berchem, J., El-Alaoui, M., and Schriver, D.: Embedding particle-in-cell simulations in global magnetohydrodynamic simulations of the magnetosphere, J. Plasma Phys.,

85, 905850109, https://doi.org/10.1017/s0022377819000072, 2019.

Wang, Y.: POS model: A Time-Dependent Three-Dimensional Magnetopause Model (1.2), Zenodo [code], https://doi.org/10.5281/zenodo.15162611, 2025.

Wang, C. and Branduardi-Raymont, G.: Progress of Solar Wind Magnetosphere Ionosphere Link Explorer (SMILE) Mission, Chinese Journal of Space Science, 38, 657–661, https://doi.org/10.11728/cjss2018.05.657, 2018.

Wang, Y. and Chen, C. X.: Numerical Simulation of Radial Plasma Transport in the Saturn's Magnetosphere, Chinese J. Geophys., 51, 635–642, https://doi.org/10.1002/cjg2.1235, 2008.

Willis, D. M.: Structure of the magnetopause, Rev. Geophys., 9, 953–985, https://doi.org/10.1029/RG009i004p00953, 1971.

Zong, Q., Escoubet, P., Sibeck, D., Le, G., and Zhang, H.: Dayside Magnetosphere Interactions, in: Dayside Magnetosphere Interactions, Geophysical Monograph Series, 303–306, https://doi.org/10.1002/9781119509592.ch17, 2020.

Remarks from the language copy-editor

Remarks from the typesetter